Flight Test of a Half-Scale Unmanned Air Vehicle

R. M. Howard,* J. C. Tanner,† and D. F. Lyons‡
Naval Postgraduate School, Monterey, California 93943

A half-scale unmanned air vehicle was flight tested to provide lift and drag data for correlation with the full-scale vehicle. Additional work was carried out to determine if wing drag could be reduced with an improved surface finish and a trailing-edge modification. Ground tests for power and thrust using a torque stand and a low-speed wind tunnel supported the flight tests for the determination of engine and propeller parameters. A panel method was used to predict the induced drag behavior of the tested air vehicle. Parasite drag was predicted by build-up methods. The predicted parasite drag for the half-scale fell short of flight-tested values by about 25%, but that predicted for the full-scale vehicle correlated well with the flight data. Within the scatter of data, the induced drag correlated satisfactorily. A comparison was made to lift and drag data extracted from full-scale, idle-power glide tests, and correlation was poor. Implications are that residual thrust prevents these glide-test data from accurately representing the full-scale drag polar.

Nomenclature

C_D = air vehicle drag coefficient
C_L = air vehicle lift coefficient
C_{Te} = effective thrust coefficient
D = air vehicle drag
d = propeller diameter
e = Oswald efficiency factor
J = advance ratio, V_∞/nd
L = air vehicle lift
n = engine speed, rps
P_r = power required
Q = engine torque
T_e = effective thrust
V_∞ = true airspeed, true flight speed
η = propeller efficiency
ρ = air density

Introduction

UNMANNED air vehicles (UAVs) have become an integral part of modern warfare. The ability to obtain timely intelligence over the horizon and to perform missions such as electronic deception, visual identification and laser designation of targets, and bomb damage assessment has been a crucial factor in the success of military operations in the recent past.

The U.S. Navy is currently fielding a UAV system in fleet operations. The Pioneer UAV is being used for gunfire spotting and for ocean surveillance and reconnaissance. A result of the urgency for a UAV system in the fleet was concurrent, rather than prior, testing of the air vehicle. The advantage of the concurrent program was that the UAV system could be integrated into the fleet quickly; the disadvantage was that subsequent problems could arise in operational use that had not yet been fully explored in the test and evaluation process.

Operational use and testing by the Unmanned Air Vehicle Office at the Pacific Missile Test Center[1,2] have indicated problems that warrant further investigation. These include the following: 1) discrepancies in predicted with flight-tested rate-of-climb, time-to-climb, and fuel flow at altitude; 2) apparent autopilot-related pitch instability; 3) tail boom structural failure; 4) severely limited lateral control; 5) slow pitch response causing degraded maneuverability at high gross weights; and 6) insufficient testing to determine the effects of the new wing on flight endurance.

In response to the need for a more complete engineering analysis of the Pioneer UAV, and for future systems in general, a program was started at the Naval Postgraduate School for flight-test research of small UAVs. This article describes the initial work of that program: to correlate performance flight data with numerical predictions in order to determine if a half-scale vehicle is suitable for analyzing problems identified for the full-scale aircraft. Such scaled-vehicle testing might prove to be beneficial for this class of military aircraft, due to the limited number of full-scale UAVs available for testing and their high cost. Precedent has been set in scaled-vehicle testing, as noted by the efforts at NASA Dryden and NASA Langley Research Centers.[3,4]

Research Program

A half-scale Pioneer UAV was acquired and is shown in Fig. 1. The half-scale Pioneer was manufactured for training purposes for the U.S. Navy and the U.S. Marine Corps. The aircraft has a span of 8.2 ft and a gross weight of 28 lb. The wing aspect ratio is 9.0 and the wing loading is 3.7 lb/ft^2. The configuration is a pusher-propeller, twin-boom arrangement made of composite materials. The aircraft is powered by an 18-cm^3 two-stroke, glow-plug engine rated at 3 hp at 16,000 rpm. The engine drives a 14-in.-diam, 6-in.-pitch propeller. The full-scale vehicle has a span of 16.9 ft, a maximum gross weight of 419 lb, and a 26-hp engine. Since the half-scale aircraft is not scaled for weight and moments of inertia, only aerodynamic coefficients are considered; no dynamic response studies were carried out.

The flight research program included torque tests for power measurements, wind-tunnel tests for propeller characteristics, and air-vehicle flight tests. Each part of the program will be briefly described.

Torque Tests

An engine torque stand was constructed to measure the power characteristics of the aircraft engine and of the electric motor used in the wind-tunnel tests. The engine mount bolted to a face plate attached to a shaft, which could freely rotate on thrust bearings. Attached to the face plate was a torque arm;

Received May 24, 1990; presented as Paper 90-1260 at the AIAA/SFTE/DGLR/SETP 5th Biannual Flight Test Conference, Ontario, CA, May 21-24, 1990; revision received Aug. 6, 1990; accepted for publication Sept. 7, 1990. This paper is declared a work of the U.S. Government and is not subject to copyright protection in the United States.

*Assistant Professor, Department of Aeronautics and Astronautics. Senior Member AIAA.
†Graduate Student; Lieutenant, U.S. Navy.
‡Graduate Student; Captain, U.S. Marine Corps; currently, Consultant, S/D Aero Engineers, 5 Truman Road, Havelock, NC 28532.

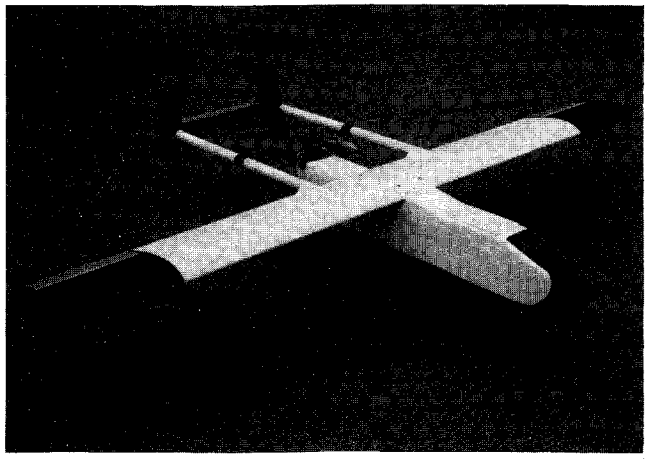

Fig. 1 Half-scale Pioneer unmanned air vehicle.

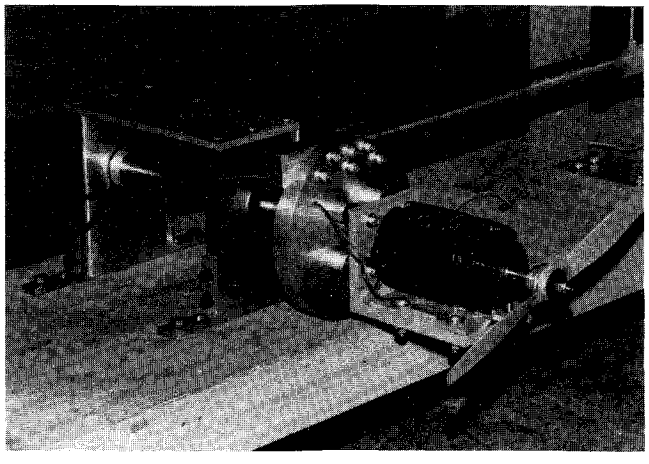

Fig. 2 Torque stand and electric motor.

forces were measured at the end of the torque arm by a massive platform scale, resolving 0.01 lb. The platform scale was used because of its inertial damping characteristics. The electric motor mounted on the torque stand is shown in Fig. 2.

Under a load, the engine tends to rotate. The torque developed is then the force at the end of the torque arm times the arm length. Different propellers were used to vary the applied loads. Measured were engine rpm and voltage input to the motor. As the shaft brake horsepower (SBHP) is solely a function of the rpm and the torque developed at the applied load:

$$\text{SBHP} = 2\pi \cdot n \cdot Q \tag{1}$$

a knowledge of the voltage input and the rpm during the wind-tunnel tests gave the identical shaft power as determined on the torque stand. Propeller efficiencies could then be determined from power and thrust data from the wind-tunnel runs. For more information on power measurements, see Refs. 5–7.

Wind-Tunnel Tests

Propeller characteristics were determined from a wind-tunnel study using a shortened model of identical frontal view as the flight vehicle. The fore and side views of the wind-tunnel model are shown in Figs. 3. Because the flight vehicle is a pusher-propeller configuration, propeller characteristics are much more sensitive to the flowfield environment than would be a tractor-propeller configuration. The wakes shed from the fuselage, wing, and engine must be modeled for a proper determination of thrust coefficients and propeller efficiencies.

The study was performed in the Naval Postgraduate School 3.5 × 5-ft wind tunnel. The complete vehicle could not be installed in the tunnel; therefore, a model was constructed with a shortened fuselage and reduced wingspan. The fuselage was made of fiberglass using the actual vehicle as a male mold, with the fore and aft sections being joined by a short center section. The wing span was set at 30 in. in order to include the wake disturbance but without introducing the wingtip vortices into the disk plane. The fuselage cross section and the wing chord were full scale. The engine cylinder was reproduced to scale, and the actual muffler was attached. In this manner, blockage effects in the propeller-disk plane could be properly modeled. As tunnel speeds were similar to flight speeds, Reynolds numbers were effectively duplicated. The only approximation was the shortened length of the fuselage and the reduced distance from the wing to the propeller, which would result in slightly thinner wake thicknesses than under actual flight conditions.

Because of the exhaust and fire hazards of running an internal-combustion engine in a closed-circuit wind tunnel, as well as problems of vibration, an electric motor was used for the wind-tunnel tests. A thrust stand was constructed to support the model and to measure the resolved force in the thrust-drag direction. The beam balance, which can be seen supporting the model in Fig. 3a, has a four-arm active bridge located in a cutout window of the vertical support. Because of the effect of the engine torque on the thrust readings, the balance calibration included a correction for the engine torque. Runs were conducted at various tunnel airspeeds and engine speeds for the determination of power and thrust as functions of advance ratio. For more information on the wind-tunnel instrumentation, see Ref. 8.

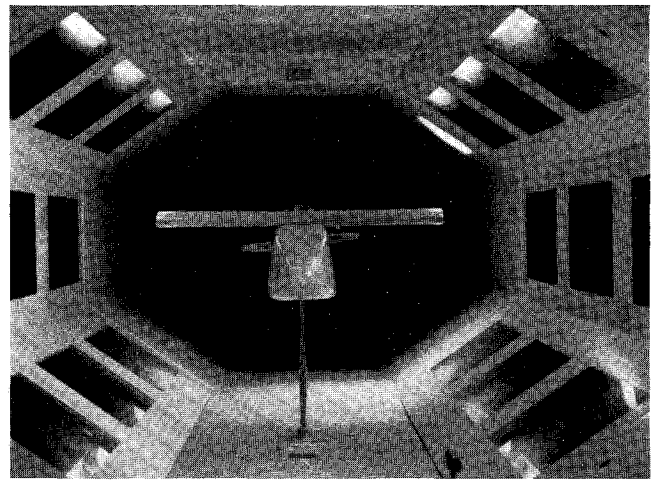

Fig. 3a Front view of wind-tunnel model.

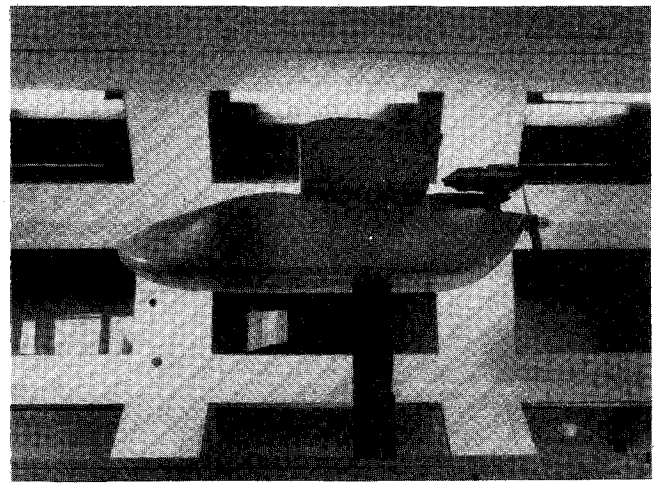

Fig. 3b Side view of wind-tunnel model.

The effective thrust coefficient and propeller efficiency were the desired parameters from the wind-tunnel tests. The effective thrust is the net thrust for the given installation; it is the thrust of the propeller in the presence of the body minus the drag with the propeller removed.[9]

The effective thrust coefficient is defined from the measured effective thrust:

$$C_{Te} = T_e/(\rho n^2 d^4) \tag{2}$$

Propeller efficiencies are determined as the ratio of the power required to the shaft brake horsepower:

$$\eta = P_r/\text{SBHP} = T_e \cdot V_\infty/\text{SBHP} \tag{3}$$

Flight Tests

Flights were performed at Fritzsche Army Airfield at nearby Fort Ord, California. The flight vehicle was equipped with a small recorder onboard to record engine rpm. A magnetic pickup supplied a voltage signal from the passage of a thin steel rod attached to the drive washer behind the propeller for the rpm measurement. A voice recorder was used for later correlation of the measured times and appropriate rpm measurements. Flight Reynolds number based on chord was about 5×10^5. Full-scale Reynolds numbers are from 1 to 1.5×10^6.

Because the flights were the first ones performed with the vehicle, minimal instrumentation was available. Airspeed was determined by the ground-speed course method,[10] as might be used for an airspeed calibration test for a new light aircraft. Steady, level 1-g flights were made over a 1500-ft distance in both directions, with the heading held and the plane allowed to drift with any crosswind. Times were recorded for the two runs for each throttle setting. In this manner, the effects of crosswinds and headwinds on resulting true airspeed could be removed. In actual practice, it was found to be difficult to track a heading other than the ground-course heading. Flights were made in the early morning when winds were light or not present. Wind speed and direction were noted, and estimations indicated that any discrepancy was well within the accuracy of the method. An engineer's transit was used to measure the vertical angle to determine height above the ground; altitudes of 60–85 ft were held during the runs.

The recorded signals were conditioned and played back through a frequency counter, and the resulting values of rpm were correlated with the average speeds for each set of two runs. Values of lift coefficient were determined from the test weight based on estimated fuel onboard and the test airspeeds. Drag coefficients were calculated from thrust, which was determined from the thrust coefficient curve for the known advance ratio.

A second method was considered for the determination of aircraft drag. Since power curves as functions of percent throttle and rpm were available, a record of throttle position and rpm would result in a value of SBHP. With the propeller efficiency determined from the advance ratio, a value for T_e and, therefore, drag could be calculated from Eq. (3). In practice, this power approach proved to be more difficult than the thrust method. Identical throttle settings for the engine on the torque stand and in the aircraft required careful calibration of throttle linkages and carburetor adjustments. Because of the simplicity of using only propeller information (C_{Te}) rather than both propeller and engine data (SBHP and η), it was decided to use the thrust method.

Wing Modifications

Both the full-scale and half-scale Pioneer use wings of relatively high aspect ratio of glass cloth/resin construction, with blunt trailing edges. The wing surfaces are exposed glass weave painted a mat gray, resulting in a rough finish. The wing trailing edge of the half-scale was 3.5% chord in thickness; that of the full-scale was not measured. Because of the amount of exposed wing surface area, and the fact that a long endurance time is of great importance to the mission of the air vehicle, it was desired to see if any noticeable improvement could be gained by reducing the trailing-edge thickness and improving the quality of the wing surface. The fuselage surfaces of the half-scale are already smooth from being constructed from a female mold, unlike the wing. The full-scale has an aluminum-skinned fuselage.

The half-scale Pioneer uses the Clark-Y airfoil, whereas the full-scale vehicle uses the NACA 4415. The two airfoils give relatively identical performances at their respective Reynolds numbers.[11] Some airfoils, the 4415 included, were designed with slightly blunt trailing edges.[12] The designed trailing-edge thickness for the NACA 4415 is 0.3% chord, although the value as constructed (for the half-scale) is 10 times that. Material was added to the trailing edge to continue the airfoil contour and bring the thickness at the trailing edge to less than 1%. This modification increased the chord by 9% and dropped the aspect ratio to 8.3. The wing surfaces were sanded, filled, and painted with a white gloss enamel paint.

It was also desired to fly the improved wing with a boundary-layer transition trip to ascertain how detrimental the original rough surface might be. Smooth and tripped conditions would give the range for changes in drag, against which the results of the original surface finish could be measured. Reference 13 discusses proper techniques for the application of transition trips. A roughness Reynolds number of 6×10^2 was used as the critical value to initiate transition.[13] Calibrated 60-grit sand was attached with double-sided tape in a narrow three-dimensional band at a distance of 1 in. from the leading edge on both upper and lower surfaces. Though neither wing section was designed to provide significant laminar flow, the results could show whether it would be effective to improve the wing surface. Perhaps the rough weave was tripping the boundary layer early, leading to higher drag, or, perhaps, at these low Reynolds numbers, the rough weave was actually beneficial in delaying laminar separation by transitioning the boundary layer and raising the effective Reynolds number, much like turbulators on model aircraft wings.

Aerodynamic Analysis

Numerical Prediction

An aerodynamic analysis of the flight vehicle was performed using an advanced low-order potential-flow panel code for the inviscid drag and a component build-up method for the viscous drag. PMARC is a nonproprietary computer program based on the widely used panel code VSAERO. The code models a three-dimensional geometry by placing a constant distribution of source and doublet singularities on quadrilateral panels of a surface geometry. A unique modeling feature of the code is its time-stepping wake, allowing aerodynamic modeling of wake roll-up and nonplanar wakes.[14]

The doublet strength on the surface panels is calculated iteratively, yielding a flow tangential to the panel surfaces. A wake is shed from the trailing edge of lifting surfaces, and the wake doublet strength is solved iteratively to satisfy the Kutta condition. Numerical differentiation is performed to obtain panel surface velocities and pressures from which the nonviscous forces and moments are calculated.

Figure 4 shows the paneled aircraft geometry. The landing gear were not included in the paneled geometry, but were considered in the drag build-up analysis. Recent studies[15,16] indicate the common use of surface-panel methods for induced drag calculations. Even so, concerns have been raised about the ability of panel-pressure methods to predict induced drag.[17] Predictions have been reported to be highly sensitive to details and density of panelization.

Though stability derivatives were also determined in this study, only the drag results are presented. Future correlations with numerical predictions will be presented as flight-test data become available.

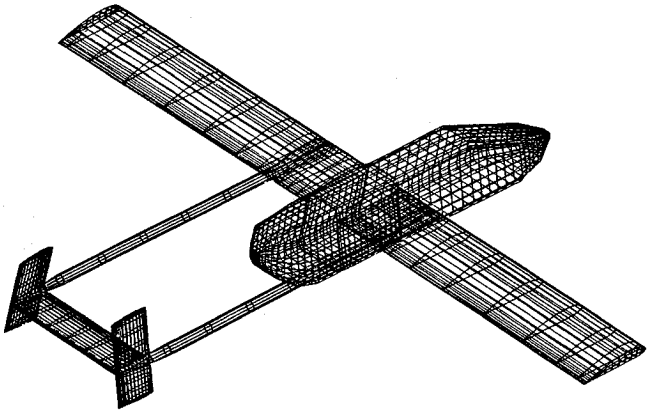

Fig. 4 Panel model of Pioneer UAV.

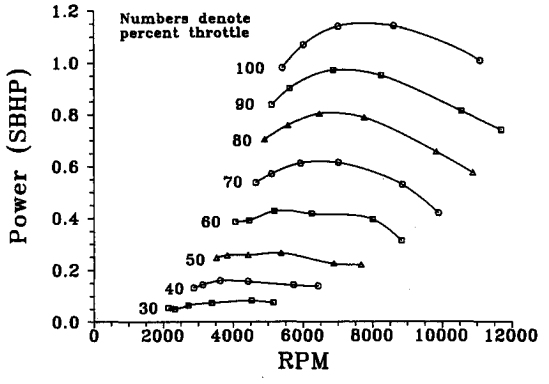

Fig. 5 Electric motor power curves.

Viscous Drag

The classical technique of Hoerner[18] to address viscous effects was applied. In this approach, a combination of theory and empirical data was used to estimate the drag contributions due to skin friction, component interference, flow separation, and surface imperfections. Included were friction drag for the wing, fuselage, booms, and tail; interference drag between the wing and fuselage and between the tail surfaces; separation drag for the fuselage, main and nose gear, booms, and engine; and drag due to control-surface gaps. For a complete review of the viscous drag breakdown, see Ref. 19.

Results

Power and Thrust

Figure 5 shows the curves generated from the torque tests for the electric motor. Also tested was the two-stroke engine used in flight; the power curves for the aircraft engine are shown in Fig. 6. Because of the notation used for the gas engine of percent throttle, the same notation was used for the electric motor, although it corresponded to a voltage setting on the motor controller. Six propellers of varying diameter and pitch were used to give the data points through which curves were fit. With the use of the curves and the throttle setting and rpm recorded during the wind-tunnel runs, the power was determined for the electric motor for the wind-tunnel test points.

From measured tunnel velocity, engine speed, and effective thrust, values of thrust coefficient were obtained and plotted vs advance ratio, as shown in Fig. 7. These data were curve fit and combined with recorded flight speed and engine rpm to result in values of in-flight thrust (and, therefore, drag). To observe the effects of the pusher configuration on η, wind-tunnel values of power and thrust were used. As can be seen in Fig. 8, maximum values of 70–75% were obtained, indicating that fuselage and wing-wake blocking was not a significant factor in degrading propeller performance. In fact, the net efficiency was probably increased over that of similar propellers in a tractor configuration due to the entrainment of air through the disk plane, which reduced the amount of separated flow behind the aft fuselage. In-flight advance ratios ran about 0.45 in the region of η of about 65–70%. Because no angle of attack was measured, no correction was made for the thrust angle above the flight path. Because no high angle-of-attack flight was made (that is, near stall), the error is taken to be negligible.

Flight Tests

Thirteen flights were conducted to gather approximately 100 test points, shown in Fig. 9. Shown is the resulting drag polar when the viscous drag prediction is added to the inviscid results of the panel-code analysis, plotted with the test points from flight test. The scatter of data is large; it is believed the large variance is due to two main causes. First, the method of measuring true airspeed brings with it timing errors due to

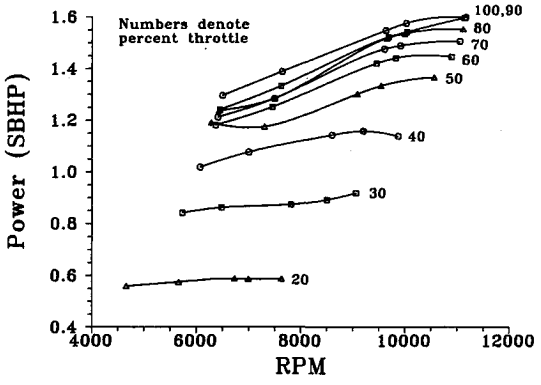

Fig. 6 Gas engine power curves.

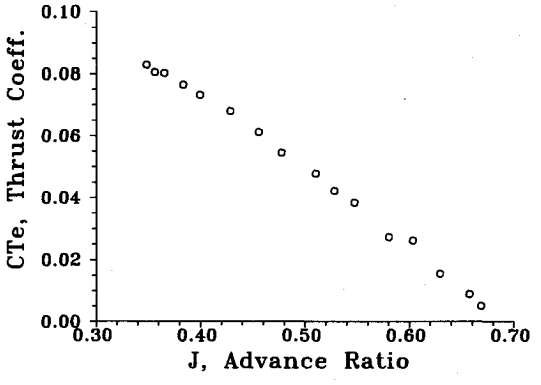

Fig. 7 Thrust coefficients for powered wind-tunnel model.

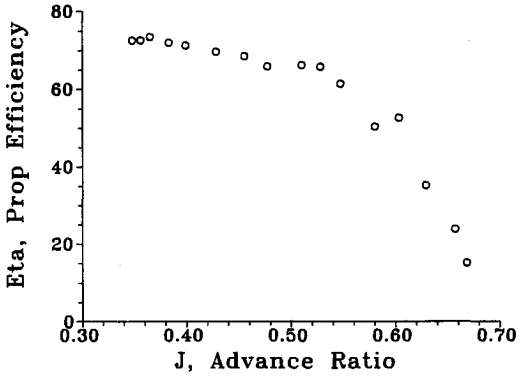

Fig. 8 Propeller efficiencies for powered wind-tunnel model.

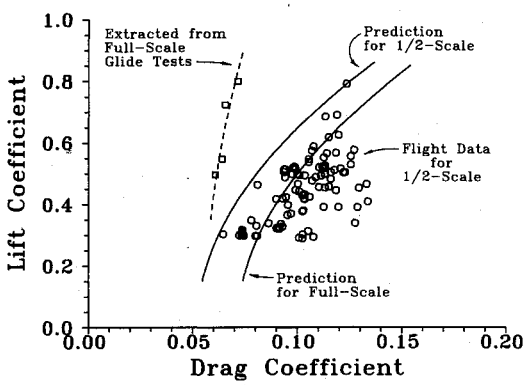

Fig. 9 Comparison of predicted drag to flight-test results.

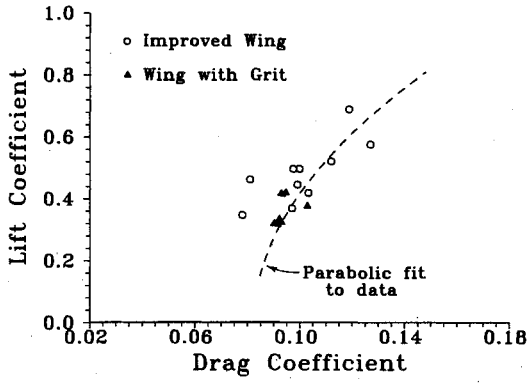

Fig. 10 Comparison of modified wing results to best fit of all flight data.

small changes in flight conditions and pilot inputs over the time of the run. An observer a few hundred feet from the test ground course noted small changes in altitude as the aircraft passed from one marker to the other. Holding a constant altitude was determined solely by eye, with a height above the runway being held of about 75 ft. Second, an error analysis indicated that a small change in the recorded rpm results in a large change in the determined thrust coefficient and, therefore, drag coefficient. Though broad, the band of scatter seems to parallel drag data collected by other investigators in performing similar work on a small UAV.[20]

Plotted with the flight data are the numerical prediction and viscous drag build-up results and values determined from idle-power glide tests for the full-scale vehicle.[1] The viscous drag predicted for the full scale is higher than that predicted for the half-scale due to the higher Reynolds number (for skin-friction drag) and the added devices such as antenna, catapult guides, position lights, and camera bubble. The numerical prediction for the full scale fits the data fairly well, whereas that for the half-scale is underpredicted. The assumption of partial laminar flow at the flight Reynolds number, as well as poor drag prediction of the gear and exposed servos, may account for the half-scale drag discrepancy. As best as can be determined from a parabolic fit of the data, the prediction of induced drag is within 15%. A value for the Oswald efficiency factor e for the numerical prediction is 0.31, whereas a parabolic curve fit to the data gives a value of 0.37. Estimated L/D_{max} is about 5.5 at a C_L of 0.79, which agrees with the flight data.

Reference 1 shows the results of idle-power tests from altitude at various airspeeds performed with the full-scale vehicle to ascertain range and endurance. If no residual thrust is assumed, the weight, airspeed, altitude, and range are sufficient to determine values of lift and drag at each airspeed. Flight-path angles during the descents varied from 4.5 to 7 deg. Four data points extracted from the glide tests are shown, with a parabolic best fit. The resulting drag values are exceedingly low and the polar steep. The estimated Oswald efficiency factor is slightly >1 and the maximum L/D over 12. Apparently, the assumption of true engine idle with no residual thrust is incorrect. Though the power-off-glide method of obtaining lift and drag information is useful if cooling-drag changes and propeller effects can be accounted for, users are warned about the application of these particular data to predict range and endurance for engine-out emergencies or loiter operations.

The values for e of 0.31 or 0.37 for the tested half-scale aircraft appear to be quite low. However, a comparison to typical values shows that, though the values are lower than for some propeller-driven aircraft, values for e should not be expected to be anywhere near 1. Flight tests of two twin-engine, retractable-gear, propeller-driven aircraft at the Naval Postgraduate School have produced values of about 0.55.[21] Flight tests for a small rail-launched, pusher-propeller UAV were performed in Ref. 20; though e is not given there, a value of about 0.5 can be extracted from the presented drag polar. As noted previously, the scatter of data in that report is identical to the results of this study. The actual value of e in the current study could, of course, be somewhat in error. As flight-test lift coefficients varied mostly from 0.3 to 0.7, it is not expected that any significant change in parasite drag has taken place with a change in lift coefficient. No significant separation should be occurring at these lift coefficients. Therefore, it is expected that the numerical results should represent the induced drag well in this flight regime, and the difference between 0.31 and 0.37 is most likely due to the data scatter. As a closing note on the induced drag results, a study was performed on the inviscid drag of the Pioneer wing alone using the PMARC code. The value of e for the wing alone was predicted to be 0.94, a reasonable value for a wing of aspect ratio 9. This value of e is less than that estimated from the glide tests for the complete vehicle, implying the unreliability of using the glide-test data for drag polar estimation.

Wing Modifications

Ten test points (20 passes) were flown with the improved wing, and nine test points were flown with the grit trips applied to the wing. These data are shown in Fig. 10 along with a parabolic fit to all of the flight data. Most of the points with the grit added are clustered at low C_L values. Because this testing represented the first performed with this air vehicle with a contaminated wing, the pilot was reluctant to proceed to high lift coefficients in the low-altitude condition required for the ground-speed runs. Indications with the limited data, comparing to the parabolic fit, are that there is no conclusive benefit gained from improving the surface finish of the Pioneer wing or detriment from tripping the boundary layer. Switching to a higher performance airfoil, such as the Wortmann FX 63-137, would perhaps be beneficial, but this modification goes well beyond those considered here. The two data points at the low lift coefficients for the improved wing suggest a potential savings of 130 drag counts with the improved wing over the original and tripped conditions, but with no benefit at high lift coefficients. Perhaps a significant amount of laminar flow is attained at the flight Reynolds number for low angles of attack, whereas at higher angles, the flow transitions well forward on the wing regardless of the surface finish. More data must be gathered to draw more conclusive answers to the question of reduced drag. Work is currently underway instrumenting the air vehicle for airspeed, yaw and pitch angles, control-surface deflections, and multichannel recording.

Conclusions

A half-scale unmanned air vehicle, based on the Pioneer aircraft currently in fleet operations, was flight tested for lift and drag measurements to compare with analytic predictions and full-scale, glide-test values. Torque-stand tests and wind-

tunnel tests were performed to gather engine and propeller data for thrust prediction in flight. A panel code and drag build-up method were used to compare with flight test results. The following conclusions were reached:

1) Measurement techniques were not sufficiently accurate for proper data resolution. The data scatter band comprised about 25% of the drag values. However, the L/D_{max} is rather insensitive to the scatter; an estimated value from the data is from 5 to 6.

2) Within the limits of the data scatter, the computational prediction of induced drag was fairly good. The prediction fell about 15% too high compared to the parabolic fit of the flight data. This error is within the margin of the data scatter.

3) A drag polar extracted from glide tests of the full-scale vehicle correlated poorly with the half-scale data and prediction. The glide-test data should not be used for prediction of expected range and time aloft for engine-out emergencies or loiter operations.

4) No apparent significant benefit was gained by improving the quality of the wing surface with the Clark-Y airfoil. A benefit may be gained with a smooth surface using an improved airfoil with some amount of laminar flow, but such a modification is not expected.

Acknowledgments

The authors wish to thank the Department of Aeronautics and Astronautics of the Naval Postgraduate School for the resources to begin the UAV flight research program. The cooperation and support of Paul Donohue of the UAV Program Office at the Pacific Missile Test Center is gratefully acknowledged. The authors wish to thank Dale Ashby, Paula Lovely, and Rich Margason at NASA Ames Research Center for their assistance in the computations and graphics. Finally, the authors thank the reviewers for their helpful comments and suggestions.

References

[1]"Pioneer Short Range Remotely Piloted Vehicle Flight Test Based Aerodynamic and Engine Performance," Fleet Combat Systems Lab., Pacific Missile Test Center, Point Mugu, CA, Dec. 1987.

[2]Sandoval, H. R. (ed.), "Initial Report for Contractor Development Tests on Baseline Pioneer and Associated Modifications," Unmanned Air Vehicle Office, Pacific Missile Test Center, Point Mugu, CA, Dec. 1988.

[3]Deets, D. A., and Brown, L. E., "Wright Brothers Lectureship in Aeronautics: Experience with HiMAT Remotely Piloted Research Vehicle—An Alternate Flight Test Approach," AIAA Paper 86-2754, Oct. 1986.

[4]Yip, L. P., Robelen, D. B., and Meyer, H. F., "Radio-Controlled Model Flight Tests of a Spin Resistant Trainer Configuration," AIAA Paper 88-2146, May 1988.

[5]Sanders, M. R., "Propeller and Engine Testing for a Mini-Remote Piloted Vehicle," M.S. Thesis, Air Force Inst. of Technology, Wright-Patterson AFB, OH, March 1975.

[6]Whatley, V., Jr., "The Whatley Torque Stand," *Sport Aviation*, Vol. 31, No. 1, Jan. 1982, pp. 12–16.

[7]Black, D., "Whatley Torque Stand Addenda," *Sport Aviation*, Vol. 31, No. 4, April 1982, pp. 40–41.

[8]Tanner, J. C., "Development of a Flight Test Methodology for a U.S. Navy Half-Scale Unmanned Air Vehicle," M.S. Thesis, Naval Postgraduate School, Monterey, CA, March 1989.

[9]Nelson, W. C., *Airplane Propeller Principles*, Wiley, New York, 1944, pp. 28–29.

[10]Roberts, S. C., *Light Aircraft Performance for Test Pilots and Flight Test Engineers*, Flight Research, Inc., Mojave, CA, 1988, p. 4.16.

[11]Miley, S. J., "A Catalog of Low Reynolds Number Airfoil Data for Wind Turbine Applications," Department of Aerospace Engineering, Texas A&M Univ., Rept. PFY1278-W, College Station, TX, Feb. 1982.

[12]Abbott, I. H., and von Doenhoff, A. E., *Theory of Wing Sections*, Dover, New York, 1959, p. 412.

[13]Braslow, A. L., Hicks, R. M., and Harris, R. V., Jr., "Use of Grit-Type Boundary-Layer-Transition Trips on Wind-Tunnel Models," NASA TN-D-3579, Sept. 1966.

[14]Ashby, D. L., Dudley, M., and Iguchi, S. K., "Development and Validation of an Advanced Low-Order Panel Method," NASA TM-101024, Oct. 1988.

[15]Vijgen, P. M. H. W., van Dam, C. P., and Holmes, B. J., "Sheared Wing-Tip Aerodynamics: Wind-Tunnel and Computational Investigation," *Journal of Aircraft*, Vol. 26, No. 3, 1989, pp. 207–213.

[16]Pfeiffer, N., and Zickuhr, T., "Validation of Computational Aerodynamics Applied to General Aviation Configurations," AIAA Paper 89-2169, July 1989.

[17]Letcher, J. S., Jr., "Convergence of Lift and Drag Predictions by a Morino Panel Method (VSAERO)," *AIAA Journal*, Vol. 27, No. 8, 1989, pp. 1019–1020.

[18]Hoerner, S. F., *Fluid-Dynamic Drag*, published by the author, Midland Park, NJ, 1958.

[19]Lyons, D. F., "Aerodynamic Analysis of a U.S. Navy and Marine Corps Unmanned Air Vehicle," M.S. Thesis, Naval Postgraduate School, Monterey, CA, June 1989.

[20]Stollery, J. L., and Dyer, D. J., "Wing-Section Effects on the Flight Performance of a Remotely Piloted Vehicle," *Journal of Aircraft*, Vol. 26, No. 10, 1989, pp. 932–938.

[21]Howard, R. M., AE 4323 Flight Test Engineering Class Notes, Naval Postgraduate School, Monterey, CA, 1988–1990.